

“Tuning fork”-shaped mesogens: large hysteresis in the interdigitated layer structure in the liquid crystal phases†

Takashi Kajitani,^a Yuichi Miwa,^b Naru Igawa,^b Masaki Katoh,^b Shigeo Kohmoto,^b Makoto Yamamoto,^b Kentaro Yamaguchi^c and Keiki Kishikawa^{*b}

^aQuality Materials Science, Graduate School of Science and Technology, Chiba University, 1-33 Yayoi-cho, Inage-ku, Chiba 263-8522, Japan

^bDepartment of Materials Technology, Faculty of Engineering, Chiba University, 1-33 Yayoi-cho, Inage-ku, Chiba 263-8522, Japan. E-mail: kishikawa@faculty.chiba-u.jp

^cChemical Elemental Analysis Center, Chiba University, 1-33 Yayoi-cho, Inage-ku, Chiba 263-8522, Japan

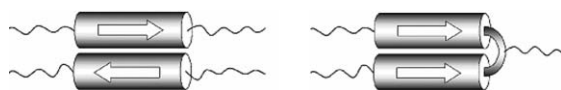
Received 23rd April 2004, Accepted 14th June 2004

First published as an Advance Article on the web 3rd August 2004

Compounds **1**, *N,N*-bis{4-[4-(4-alkoxybenzoyloxy)benzyloxy]benzoyl}alkylamines, were designed and synthesized as “tuning fork”-shaped molecules, and their properties were investigated by polarized light microscopy and differential scanning calorimetry, and the layer distances were measured by X-ray diffraction. The observed smectic A liquid crystal phases indicated the existence of large hysteresis in XRD. The multiple broad peaks of the layer distances originated in the plural extent of interdigitation of the alkyl chains between the layers, and the layer distances strongly depended on the hysteresis. Further, the chiral and racemic liquid crystalline compounds, (*R*)-**1k** and *rac*-**1k**, showed a clear difference in the interlayer interdigitations in their mesophases.

1. Introduction

The dipole–dipole interaction is one of the most important interactions to generate superstructures in mesophases. Intermolecular dipole–dipole interactions have produced a lot of highly ordered structures in liquid crystal phases: 1) bilayer smectic phases,¹ 2) re-entrant phases,² 3) chiral phases generated by achiral banana-shaped molecules,³ 4) dimerization of apolar molecules (anthraquinone derivatives) by their molecular distortion,⁴ 5) organization of bent-rod molecules possessing a central large dipole,⁵ and 6) un-even parallel association of half-disk molecules.⁶ Further, molecular dipoles greatly influence the physical properties (charge mobility,⁷ ionic conductivity,⁸ fluorescence,⁹ electro-optic switching,¹⁰ and dipole modulation by *trans*–*cis* photoisomerization¹¹) of the liquid crystals. Thus, introduction of large polarity into a molecule is one of the most important approaches for their rapid response. In addition, the generation of novel superstructures (ferroelectric alignment¹² or helical formation¹³) by controlling intermolecular dipole–dipole interactions has been predicted theoretically in mesophases. Usually, in order to generate a large molecular dipole, polar substituents (–CN, –NO₂, or –F) or linkage groups (–C=N–, –N=NO–, or –COO–) are introduced in the liquid crystalline molecules.¹⁴ However, these molecular polarities are cancelled out by having an anti-parallel arrangement (Scheme 1 left),¹⁵ and the time-averaged dimer behaves as a non-polar unit. In contrast, arrangement of two polar mesogenic cores in a syn-parallel manner by linkage



Scheme 1 Arrangement of two mesogens: (left) anti-parallel organization of two polar molecules and (right) a molecule consisting of two polar mesogenic cores in syn-parallel arrangement.

† Electronic supplementary information (ESI) available: colour version of Fig. 1 and analytical data for **1c**–**1i**. See <http://www.rsc.org/suppdata/jm/b4/b406177b/>

with a covalent bond (Scheme 1 right) prevents the cancellation, and generates a strong molecular dipole as a “tuning fork”-shaped mesogen. Though the “tuning fork”-shaped molecules also dimerize to cancel out their polarities in the mesophase, a large intermolecular dipole–dipole interaction is expected between the two molecules.

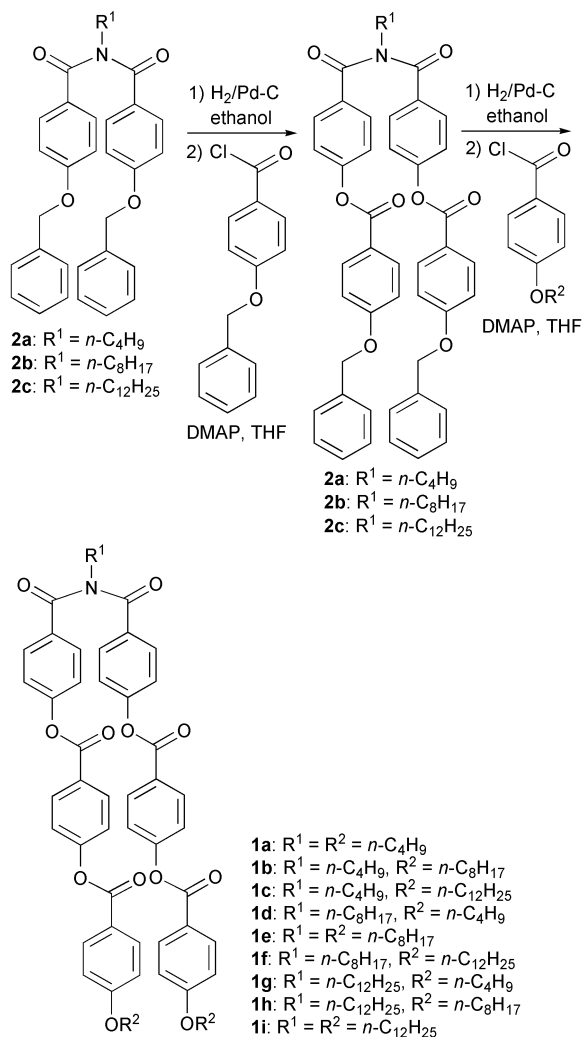
In this study compounds **1** were designed and synthesized as a “tuning fork”-shaped molecule (Scheme 2), and the properties were investigated by polarized light microscopy and differential scanning calorimetry (DSC), and the layer distances were measured by X-ray diffraction (XRD). As a result, we found that the smectic A liquid crystal phases indicated large hysteresis in XRD. The multiple broad peaks of the layer distances originated in the plural extent of interdigitation of the alkyl chains between the layers, and the layer distances strongly depended on the hysteresis.

In general, smectic phases have a periodicity in one direction to show its peculiar layer distance(s) in XRD, which is characteristic of all smectic phases and in most cases does not depend on their hysteresis because of the fluidity of liquid crystals. However, these liquid crystal phases are highly viscous and showed large hysteresis, even though these compounds are low molecular weight liquid crystalline compounds.

2. Result and discussion

The behavior of the compounds and identification of the phases

The compounds **1a**–**i** were synthesized by the method in our previous paper¹⁶ (Scheme 2). The behavior of liquid crystalline compounds **1a**–**i** is shown in Table 1. Length of the alkyl chains seems to be a main factor to determine the behavior of these liquid crystalline compounds. Compounds **1a**, **1c**, **1d**, and **1g** possessing butyl groups as the terminal chains (R¹ or/and R²) exhibited nematic phases, and very small transition enthalpies (0.030–0.071 kcal/mol) were observed for the transitions between the nematic and the isotropic liquid phases. At the transition from the isotropic liquid to the nematic phase, homeotropic textures of the nematic phases appeared simultaneously from all part of the isotropic sample.



Scheme 2 Synthesis of 1.

Compounds **1c**, **1d**, and **1g** also exhibited smectic A phases at the temperature range below their nematic phases. The transition enthalpies between the nematic and the smectic A phases were also small (0.12–0.31 kcal mol⁻¹). These small transition enthalpies indicate a similarity between the molecular aggregations before and after the transition. It is assumed that the tuning-fork molecules exist as time-averaged dimers with an antiparallel manner even in the isotropic and nematic phases. In contrast, the other compounds (**1b**, **1e**, **1f**, **1h**, and **1i**) only displayed smectic A phases over the wide temperature ranges. In all these smectic A phases, typical textures of smectic A phases, such as batonets and fan-shaped textures, appeared from their isotropic liquid on cooling (Fig. 1). The batonets which were parallel to either the polarizer or analyzer of the microscope were dark, and it meant that the long axes of the molecules were parallel with respect to the layer normal.¹⁷ From conoscopic study of the homeotropically aligned sample in the liquid crystal phase, the uniaxiality was confirmed. These observations in polarized light microscopy indicated that these liquid crystal phases belonged to smectic A phases. However, the peak shapes in DSC (Fig. 2 and Fig. 3) were different from those of usual smectic A phases of low-weight molecules, and a highly broad peak was observed in both of these smectic A–isotropic phase transitions despite the high purity of the compounds.

XRD of the smectic A phases

XRD of compounds **1b–1i** in a glass capillary (diameter: 1.5 mm) was carried out on their smectic A phases. Every

Table 1 Behavior of compound 1a–i

Compound	Behaviour ^a
1a	Cr $\xrightleftharpoons[129(-5.7)]{145(5.7)}$ N $\xrightleftharpoons[176(-0.045)]{176(0.045)}$ I
1b	Cr $\xrightleftharpoons[58(-2.0)]{99(2.2)}$ SmA $\xrightleftharpoons[180(-1.2)]{180(1.2)}$ I
1c	Cr $\xrightarrow{76(4.3)}$ SmA $\xrightleftharpoons[133(-0.29)]{133(0.31)}$ N $\xrightleftharpoons[142(-0.060)]{142(0.071)}$ I
1d	Cr $\xrightleftharpoons[71(-4.1)]{113(4.1)}$ SmA $\xrightleftharpoons[146(-0.12)]{147(0.13)}$ N $\xrightleftharpoons[161(-0.043)]{161(0.053)}$ I
1e	Cr $\xrightleftharpoons[71(-3.1)]{98(3.1)}$ SmA $\xrightleftharpoons[199(-2.3)]{199(2.4)}$ I
1f	Cr $\xrightarrow{88(3.7)}$ SmA $\xrightleftharpoons[178(-2.1)]{178(2.7)}$ I
1g	Cr $\xrightleftharpoons[67(-2.4)]{104(2.5)}$ SmA $\xrightleftharpoons[157(-0.19)]{157(0.19)}$ N $\xrightleftharpoons[216(-0.030)]{216(0.041)}$ I
1h	Cr $\xrightarrow{86(3.8)}$ SmA $\xrightleftharpoons[201(-2.4)]{201(2.5)}$ I
1i	Cr $\xrightarrow{98(3.5)}$ SmA $\xrightleftharpoons[210(-2.3)]{210(2.4)}$ I

^a The transition temperatures (°C) and enthalpies (in parentheses, kcal mol⁻¹) were determined by DSC (5 °C min⁻¹) and are given above and below the arrows. Cr, N, SmA, and I indicate crystal, nematic, smectic A, and isotropic phases, respectively.

compound showed several broad peaks in the small angle region (Table 2) except compounds **1f** ($R^1 = n\text{-C}_8\text{H}_{17}, R^2 = n\text{-C}_{12}\text{H}_{25}$) and **1i** ($R^1 = R^2 = n\text{-C}_{12}\text{H}_{25}$) which showed one peak in each of their small angle regions corresponding to its molecular length. Fig. 4 and Fig. 5 show the XRD patterns of **1b** ($R^1 = n\text{-C}_4\text{H}_9, R^2 = n\text{-C}_8\text{H}_{17}$) and **1d** ($R^1 = n\text{-C}_8\text{H}_{17}, R^2 = n\text{-C}_4\text{H}_9$), respectively.

Estimation of the intermolecular dipole–dipole interactions by MM2, AM1, and single crystal XRD

MM2 calculation¹⁸ of **1a** indicated that the two mesogenic cores were parallel and contacted each other in the most stable conformation, because of the intramolecular interactions

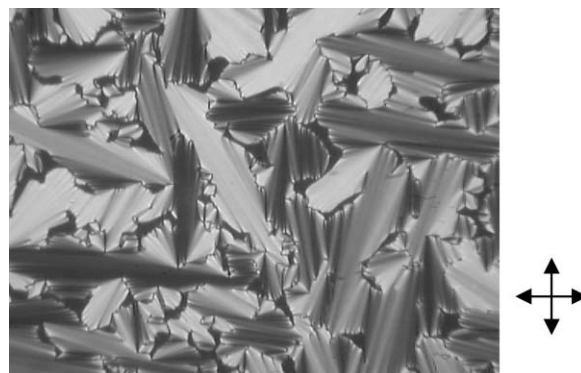


Fig. 1 A polarized optical micrograph of **1e**. Fan-shaped textures at 114 °C on cooling ($\times 400$). The directions of the crossed polarizers are indicated by the arrows. The dark lines are parallel to the directions.

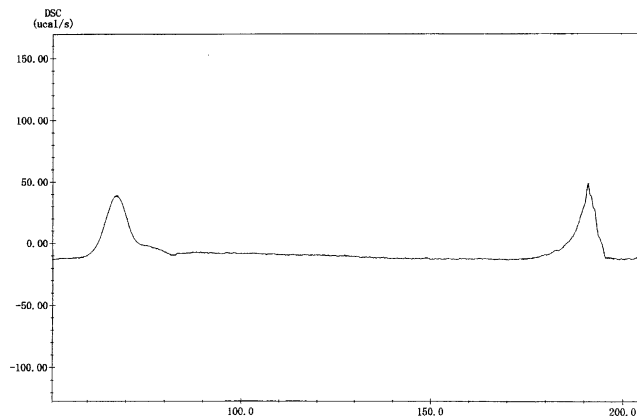


Fig. 2 DSC chart of **1e** on cooling. Cooling rate: $5\text{ }^{\circ}\text{C min}^{-1}$.

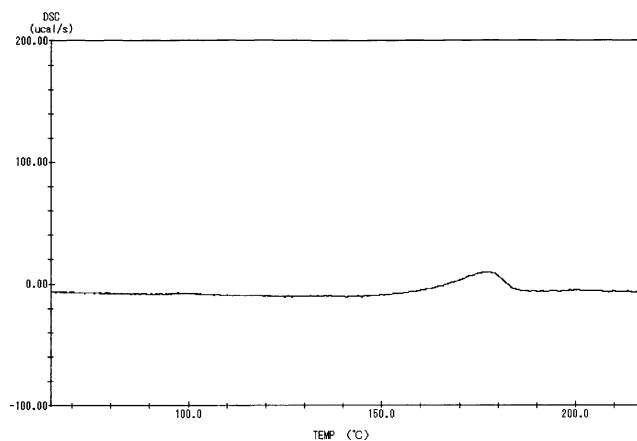


Fig. 3 DSC chart of **1f** on cooling. Cooling rate: $5\text{ }^{\circ}\text{C min}^{-1}$.

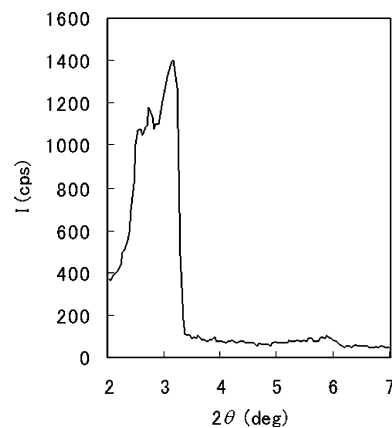


Fig. 4 XRD of **1b** in a capillary method at $120\text{ }^{\circ}\text{C}$ (liquid crystal phase).

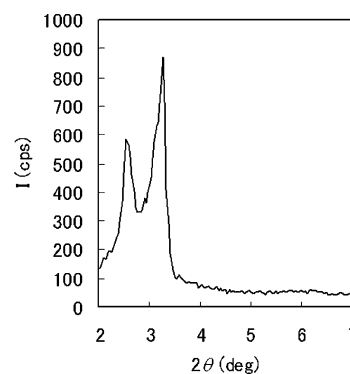
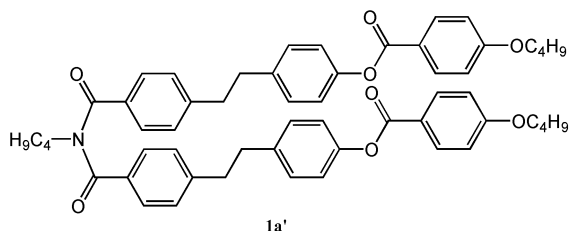
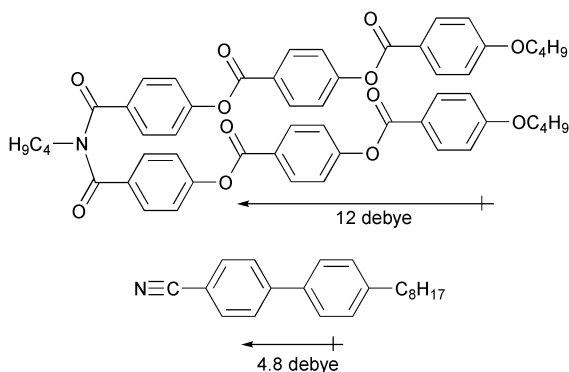


Fig. 5 XRD of **1d** in a capillary method at $120\text{ }^{\circ}\text{C}$ (liquid crystal phase).

Table 2 The $d(100)$ peaks in XRD data of the smectic A phases^a

Entry	Compound	R ¹	R ²	temp/ $^{\circ}\text{C}$	$d(100)/\text{Å}$			Molecular length/ Å ^b	
1	1b	$n\text{-C}_4\text{H}_9$	$n\text{-C}_8\text{H}_{17}$	100	34.5	30.7	29.4	35	
				120	34.5	32.5	27.9		
				140	35.0	32.0	27.9		
				160	35.0	31.5	28.3		
2	1c	$n\text{-C}_4\text{H}_9$	$n\text{-C}_{12}\text{H}_{25}$	100	48.0	42.4	38.7	40	
				110	46.0	40.9	37.4		
				120	45.9	40.9	36.8		
				130	44.1	40.9	39.4		
3	1d	$n\text{-C}_8\text{H}_{17}$	$n\text{-C}_4\text{H}_9$	120	35.0	27.2	35		
				130	34.5	27.2			
				140	32.0	27.6			
4	1e	$n\text{-C}_8\text{H}_{17}$	$n\text{-C}_8\text{H}_{17}$	100	38.1	33.4	40		
				110	37.4	33.4			
5	1f	$n\text{-C}_8\text{H}_{17}$	$n\text{-C}_{12}\text{H}_{25}$	90	49.0		45		
				100	48.0				
				150	46.0				
6	1g	$n\text{-C}_{12}\text{H}_{25}$	$n\text{-C}_4\text{H}_9$	140	41.6	39.4	36.2	40	
				150	40.9	38.7	36.2		
				160	42.4	38.1	36.2		
				180	45.0	37.4			
7	1h	$n\text{-C}_{12}\text{H}_{25}$	$n\text{-C}_8\text{H}_{17}$	140	46.0			45	
				150	45.0	37.4			
				160	45.0	38.1			
				180	45.0	41.6	39.4		38.1
				190	41.6	37.4			
8	1i	$n\text{-C}_{12}\text{H}_{25}$	$n\text{-C}_{12}\text{H}_{25}$	140	50.2			50	
				150	50.2				
				160	48.0				
				170	46.0				
				180	49.0				

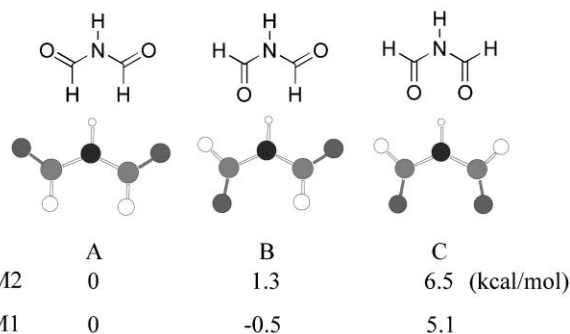
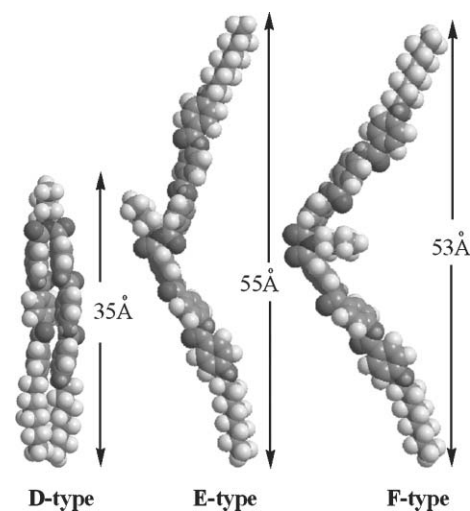
^aThe XRD was measured by a capillary method on the first heating. The temperature ratio was $5\text{ }^{\circ}\text{C min}^{-1}$ and the temperature was maintained during each XRD measurement. ^bThe molecular lengths were calculated by molecular modeling, based on the "tuning-fork" conformation.

Scheme 3 Compound **1a'**.Scheme 4 Dipole moments of compound **1a** and 8CB.

between the two cores. In the case of compound **1a'**¹⁶ (Scheme 3) which showed a nematic liquid crystalline phase, the parallel arrangement of the two mesogenic cores was observed in X-ray structural analysis of the single crystal. The intramolecular CH/ π interactions¹⁹ between those benzene rings ($C_{Ar} \cdots C_{Ar}$: 3.81–3.94 Å) and C=O/C=O interactions²⁰ between the two esters ($C=O \cdots C=O$: 3.38 Å) were estimated from the interatomic distances and the spatial arrangement of their moieties. Further, dimerization of the “tuning fork”-shaped molecules in an anti-parallel manner was also confirmed in the crystal packing diagram. Furthermore, in most cases (**1b**, **1d**, **1e**, **1g**, **1h** and **1i**), XRD of the liquid crystal phases gave the peaks of the layer distances corresponding to their molecular lengths which were calculated based on the “tuning fork”-shaped conformations. A large dipole moment (12 debye) is indicated by AM1 calculation²¹ for the “tuning fork”-shaped conformation of **1a** in the direction of the long axis (Scheme 4). Time-averaged dimerization has been known for 4'-alkyl and 4'-alkoxy-4-cyanobiphenyls,²² and in the case of 4-cyano-4'-octylbiphenyl (8CB in Scheme 4) the dipole moment was only 4.8 debye in AM1 calculation. The dipole moment of **1a** (12 debye) is 2.5 times larger than that of 8CB. Accordingly, movements of the molecules in the direction of their long axes seem to be strongly prevented by the strong intermolecular interaction with the neighboring molecules in the layer.

Conformation of **1** in the liquid crystal phase

To investigate the most stable conformation of the connecting part CO–N–CO, the relative formation energies of three *N,N'*-diformylamine conformers **A**, **B** and **C** were calculated by MM2 and AM1 (Fig. 6). Conformer **C** was the least stable of the three conformers because of the strong electrostatic repulsion between the two carbonyl oxygen atoms. Conformer **A** and **B** indicated similar values in the formation energies. Based on the three conformations, the molecular lengths of the conformers of **1b** (**D**, **E** and **F** in Fig. 7) were calculated by MM2 to give 35, 55 and 53 Å, respectively. If the packing force in the liquid crystal phase is sufficient to overwhelm the electrostatic repulsion between the two mesogenic units in the molecule, it can be presumed that the molecule has the most

Fig. 6 Relative energy levels of *N,N'*-diformylamine in MM2 and AM1 calculations.Fig. 7 Three stable conformations of **1b**. Tuning-fork (**D**-type), asymmetric bent-rod (**E**-type), and symmetric bent-rod (**F**-type) shapes.

compact conformation, the **D**-type. If the packing force is not sufficient to overwhelm the electrostatic repulsion, the molecule may have the bent conformations, the **E**- and **F**-types. In conformer **D**, both R^1 and R^2 directly influence the layer distance of the smectic A phase. On the other hand, in conformers **E** and **F**, R^2 length directly influences the layer distance, but R^1 length does not. From Table 2, it was obvious that both R^1 and R^2 influenced the observed layer distances. For example, compounds **1b** and **1d** which have the same molecular lengths (35 Å) showed similar layer distances (**1b**: 34.5–35.0 and **1d**: 32.0–35.0 Å) despite the different lengths of the R^2 groups. In the cases of **1b**, **1e**, and **1h**, the R^2 group is the same length (*n*-C₈H₁₇), however, the longest layer distance in each compound (**1b**: 34.5–35.0, **1e**: 37.4–38.1, and **1h**: 41.6–46.0 Å) is almost proportional to its molecular length calculated as the tuning-fork conformation (**1b**: 35, **1e**: 40, and **1h**: 45 Å). Accordingly, the tuning fork conformation (**D**-type) was not contradictory to the layer distances observed in the liquid crystal phases. To investigate the correlation between the molecular length and the layer distance, each layer distance in all the compounds was plotted against the molecular length based on the tuning fork (**D**-type) and asymmetric bent (**E**-type) models (Fig. 8 and Fig. 9). The solid line shows that the layer distance equals the molecular length. The broken and dotted lines corresponds to layer distances 5 Å longer and 5 Å shorter than the molecular length, respectively. The observed layer distances fit within the range of 5 Å from the molecular length in the **D**-type model (Fig. 8), while large differences arise in the **E**-type model (Fig. 9). These results also provide further evidence that the molecules have the tuning-fork conformation in the liquid crystal phase.

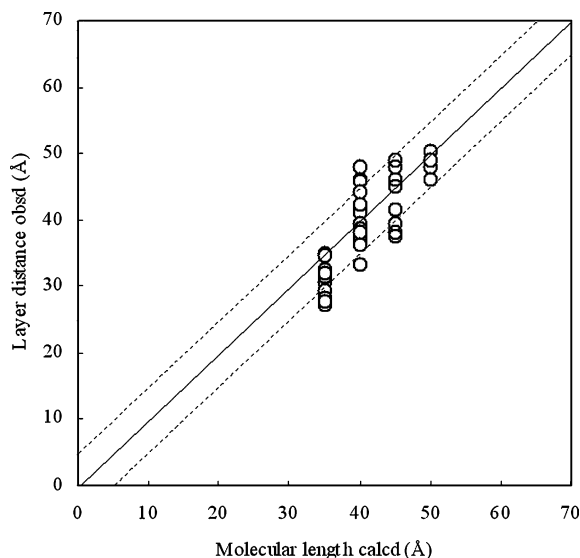


Fig. 8 The layer distance and the molecular length based on the tuning-fork model (**D**-type). The solid, broken, and dotted lines correspond to the layer distances equal to the molecular length, the molecular length + 5 Å, and the molecular length - 5 Å, respectively, in the tuning-fork model (**D**-type).

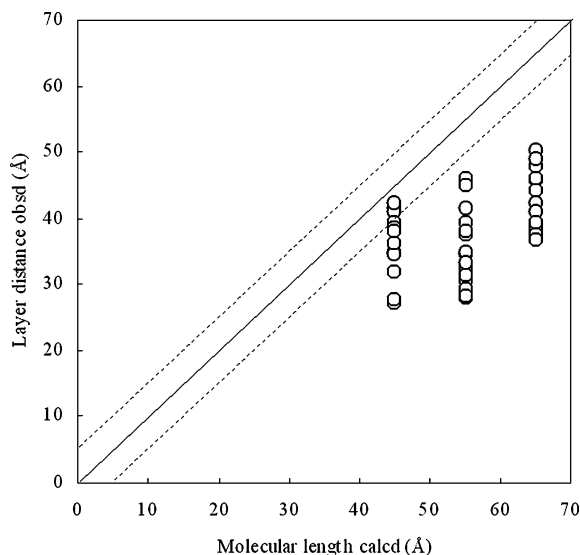


Fig. 9 The layer distance and the molecular length based on the asymmetric bent model (**E**-type). The solid, broken, and dotted lines correspond to the layer distances equal to the molecular length, the molecular length + 5 Å, and the molecular length - 5 Å, respectively, in the asymmetric bent model (**E**-type).

XRD of the pressed samples

The liquid crystalline samples were spread on a glass plate using another glass plate to give thin layered samples which exhibited homeotropic textures. The samples on the plates were measured under atmospheric pressure. Both **1b** and **1d** showed sharp [100] peaks at 2.82 (31.3 Å) and 2.98 (29.6 Å), respectively (Fig. 10 and Fig. 11). It was confirmed that the pressure in the spreading could generate the well-aligned and compressed layer structure. The homeotropic texture indicated that the averaged direction of the cores was parallel to the layer normal and the layers were parallel to the plate. The decrease of the layer distances indicated interdigitation between the alkyl layers in the direction of the layer normal. The decreased length (4–5 Å) corresponded to the length of the butyl group (*gauche*-form: 4.5 and all-*trans*-form: 5 Å). It was assumed that the decrease originated in the interdigitation between the R^1 (**1b**:

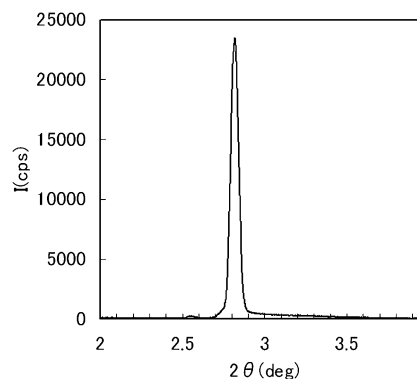


Fig. 10 XRD of **1b** in a thin layer method at 120 °C.

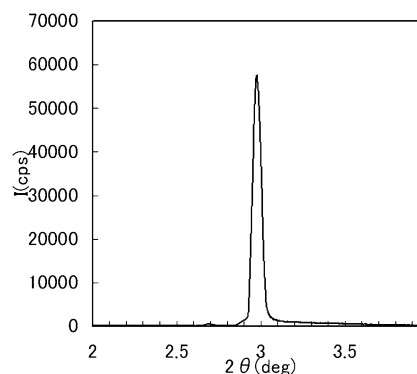


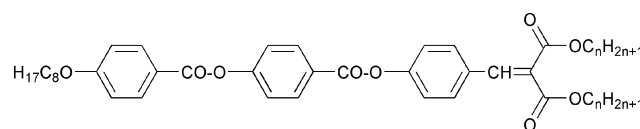
Fig. 11 XRD of **1d** in a thin layer method at 120 °C.

butyl, **1d**: octyl) and R^2 (**1b**: octyl, **1d**: butyl) groups in the tuning-fork conformation.

Similarity between swallowtail compounds and **1**

The broad temperature range of the smectic A phase may also bear out the most compact conformation (**D**-type). To the best of our knowledge, such a stable smectic A phase has not been reported for bent molecules (**E**-type). In addition, in the case of swallow tail molecules in the smectic A phase (Scheme 5), the interdigitated layer distance has been reported with the layer distance corresponding to the molecular length.²³ The rod-like molecule has three normal alkyl groups as the terminal chains, and has an α,β -dicarbonyl as the bi-forked junction. The α,β -dicarbonyl moiety also has three stable conformers, but they concluded that the aliphatic double chains must be parallel to each other in order to explain the increase of the layer distance with the number of carbon atoms in the normal alkyl chain. From these similarities, it was natural to conclude that our molecules also had the tuning-fork conformation in the liquid crystal phase.

From the molecular packing diagram, the conformational calculations, the XRD experiment of the pressed samples, the correlation between the layer distance and molecular length, and the similarity to the swallowtail mesogen, the tuning-fork (**D**-type) was most likely as the molecular conformation in the liquid crystal phase. This indicated that the packing forces were sufficient to overwhelm the intramolecular electrostatic repulsion between its two mesogenic cores.



Scheme 5 Swallowtail molecule (ref. 23).

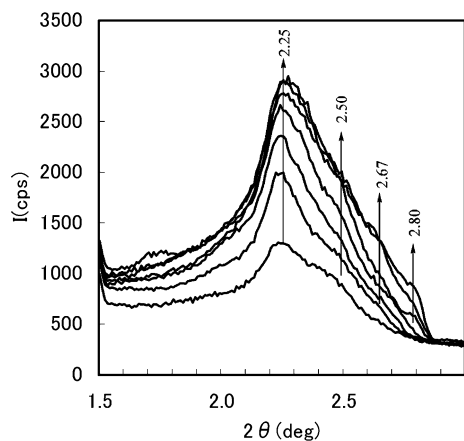


Fig. 12 Growth of the liquid crystal domain of **1b**. XRD was measured at 183, 171, 160, 149, 138, 126, and 114 °C on cooling (from the bottom to the top). The arrows indicate growth of the peaks. The cooling rate was 5 °C min⁻¹.

Monitoring of growth of the liquid crystal domains by XRD

Growth of the liquid crystal domains from the isotropic liquid was monitored by XRD in the cases of **1b** and **1e**. On cooling, growth of their plural peaks was observed. The small angle region (1.50–3.00°) of XRD was measured for **1b** on cooling from 183 to 114 °C (Fig. 12). First, the two peaks at 2.25 (39.2 Å) and 2.50 (35.3 Å) grew, and then the two peaks at 2.67 (33.1 Å), and 2.80 (31.5 Å) came out. The intensity of these peaks increased on cooling and then saturated at a certain level. In the case of **1e**, the peak at 2.00 (44.1 Å) appeared first at 183 °C, and then the peaks at 2.30 (38.4 Å) and 2.42 (36.5 Å) increased on cooling from 183 to 138 °C (Fig. 13). The longest layer distances (39.2 and 44.1 Å) observed in the monitoring experiments of **1b** and **1e** were about 4 Å longer than their molecular lengths (**1b**: 35 and **1e**: 40 Å). This indicated that these domains were generated as smectic A_d phases at the first stage on cooling, in which the molecules dimerized in an anti-parallel manner with a shift (*ca.* 4 Å) and the alkyl chains did not interdigitate between the layers, and then the interdigitated layers occurred with cooling to give the peaks at the shorter layer lengths.

In the case of **1e**, after heating and maintaining the temperature at 150 °C for two hours, no measurable change was observed in the peak positions and intensities in the XRD chart, though the temperature (150 °C) was almost the middle of the temperature range of the smectic A phase (98–199 °C on heating and 193–71 °C on cooling) and high enough to remove stress in usual low molecular weight liquid crystalline

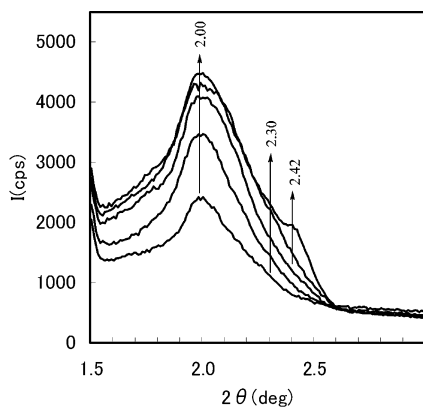
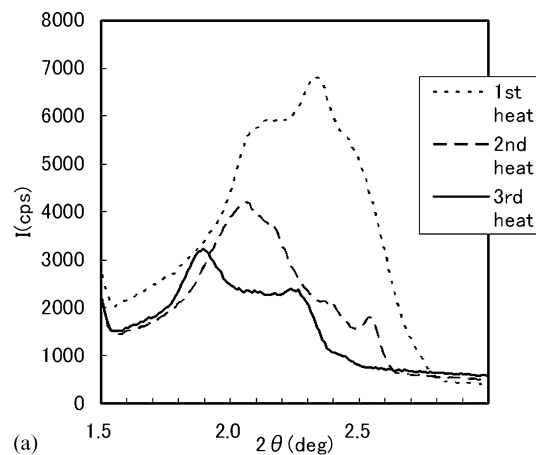
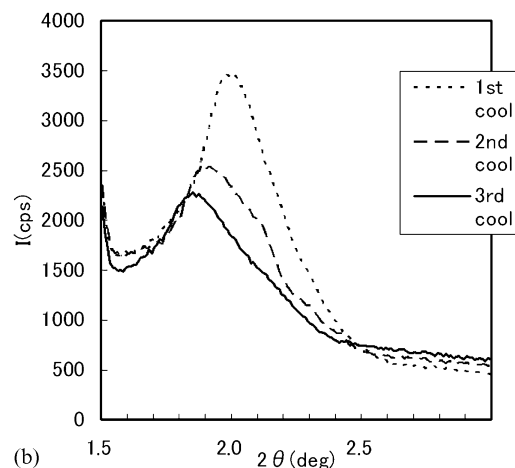


Fig. 13 Growth of the liquid crystal domain of **1e**. XRD was measured at 183, 171, 160, 149, and 138 °C on cooling (from the bottom to the top). The arrows indicate growth of the peaks. The temperature rate was 5 °C min⁻¹.



(a)



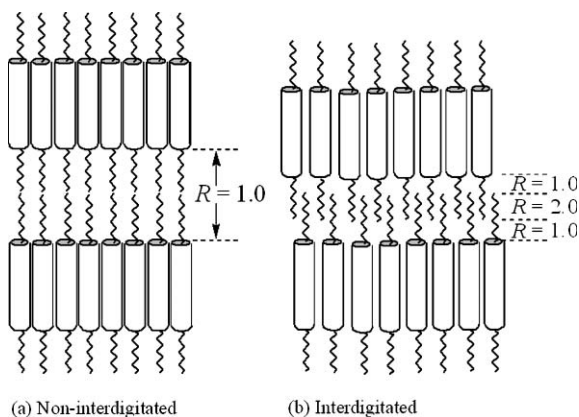
(b)

Fig. 14 (a) XRD of **1e** at 150 °C on heating. (b) XRD of **1e** at 150 °C on cooling.

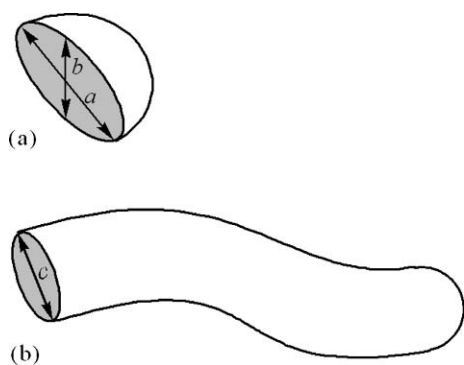
compounds. Then, the XRD patterns of **1e** were measured at 150 °C on heating and cooling (rate: 5 °C min⁻¹) in one heat–cool cycle (70 → 150 → 210 → 150 → 70 °C), and this procedure was repeated three times (Fig. 14). The peak positions and their intensities on heating are different from those on cooling. The diffraction pattern on the first heating (Fig. 14a) has peaks at 2.17 (40.7 Å), 2.34 (37.7 Å) and 2.50 (35.3 Å), while the diffraction pattern on the first cooling (Fig. 14b) has only one peak at 2.00 (44.1 Å). After the two additional heat–cool cycles, the peak intensities decreased and the peak top converged at 1.87–1.90 (*ca.* 47 Å) on both heating and cooling. The smectic A_d phase without interdigitation seems to be stable at the temperature close to the clearing point. From these results, it is clear that the multiplicity in the layer distances depended on the hysteresis of the sample.

Explanation for the interdigitation

In order to estimate the degree of interdigitation in the smectic A phase, we introduced a new coefficient (R_{clc}) as follows. In the model, the long axes of the terminal chains and the rod-like cores are parallel to the layer normal (Scheme 6). The coefficient is defined as $R_{clc} = N_{chain}/N_{core}$. In the equation, N_{chain} is the number of chains crossed by a plane which is parallel to the layer, and N_{core} is the number of rod-like cores in the layer. If the size of the plane is S_{plane} and the alkyl chains (the number is N'_{chain}) in the alkyl chain layer are packed tightly, S_{plane}/N'_{chain} nearly equals the cross section of an alkyl chain ($= S_{chain}$). If the rod-like cores (the number is N'_{core}) in the core layer are packed tightly, S_{plane}/N'_{core} nearly equals the cross section of a core ($= S_{core}$). When both the cores and chains are packed with almost no empty space, respectively, R_{clc} equals N'_{chain}/N'_{core} .



Scheme 6 Non-interdigitated and interdigitated state and R_{clc} in the case of 1-core-2-chain type compounds.

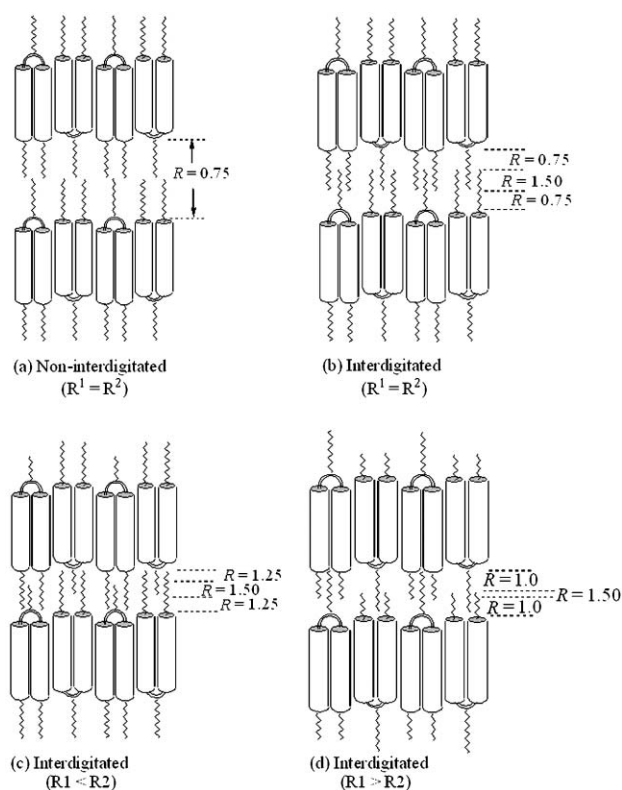


Scheme 7 Cross sections of (a) a benzene ring and (b) an alkyl chain (a : 6.3, b : 3.6, c : 4.0 Å)

Accordingly, $N'_{chain}/N'_{core} = (1/N'_{core})/(1/N'_{chain}) = (S_{plane}/N'_{core})/(S_{plane}/N'_{chain}) = S_{core}/S_{chain}$. We assume that the shapes of the cross sections of a benzene ring and an alkyl chain are an oval and a circle (Scheme 7), respectively. These areas are $6.3 \times 3.6 \times (\pi/4) (= S_{core})$ and $4.0 \times 4.0 \times (\pi/4) (= S_{chain})$ Å² at a rough estimate, which is calculated from their dimensions a – c (a : width of a benzene-ring; 6.3, b : thickness of a benzene-ring; 3.6, and c : diameter of an alkyl chain; 4.0 Å).²⁴

The obtained ratio for S_{core}/S_{chain} (1.4:1) indicated that the most adequate R_{clc} is approximately 1.4 in smectic A phases if the movements of the cores and alkyl chains are not taken into account (a temperature factor must be considered for the exact R_{clc}). For example, if one rod-like molecule has one alkyl chain at both terminals, R_{clc} is 1.0 in all levels of the alkyl chain layer in the non-interdigitated state (Scheme 6a) and 2.0 in the interdigitated part of the alkyl chain layer in the partially interdigitated state (Scheme 6b). If R_{clc} becomes larger than 1.4 with the interdigitation, the intermolecular distances between the cores increase and the core–core interaction decreases. As a consequence, the non-interdigitated state is recovered to stabilize the layer structure. If R_{clc} is much smaller than 1.4, it is assumed that interdigitation occurs to supply the lack of space in the alkyl chain layer.

In the smectic A phases of compounds **1** except **1f** and **1i**, the probability of interdigitation is explained as follows. For example, in the case of **1e** ($R^1 = R^2$), R_{clc} is 0.75 (< 1.4) at all levels of the alkyl chain layer in the non-interdigitated state (Scheme 8a), and the interdigitation of the alkyl chain layers was preferred to generate the adequate R_{clc} ($= 1.5$ (≈ 1.4)) (Scheme 8b). In the case of $R^1 \neq R^2$, the interdigitated states (Schemes 8c and d) were also preferred to achieve adequate R_{clc} in the alkyl chain layer. In the case of **1f** ($R^1 = n\text{-C}_8\text{H}_{17}$, $R^2 = n\text{-C}_{12}\text{H}_{25}$) and **1i** ($R^1 = R^2 = n\text{-C}_{12}\text{H}_{25}$) which have relatively long alkyl chains in this series, the flexible movement



Scheme 8 Non-interdigitated and interdigitated states and R_{clc} in the cases of the 2-core-3-chain type compounds.

of the long alkyl chains seems to prevent the interdigitation between the layers. The difference in the interdigitation might be observed in DSC experiments of **1e** and **1f**. In the case of **1e**, the peak from the isotropic to the liquid crystal phase had several small shoulders, while in the case of **1f** it had a single peak.

From monitoring of growth of the liquid crystal domains by XRD, it was found that the longer layer distance grew at higher temperature and the shorter distance grew at lower temperature. This can be explained by the decrease in the alkyl chain mobility on cooling, which decreases its excluded volume and increases the degree of the interdigitation between the layers. In the smectic A_d phase observed in the heat–cool cycle XRD experiment of **1e** (layer distance: 47 Å), we propose the dimerization as depicted in Fig. 15. In the dimer, it is assumed that the polar connecting groups (–N–CO–, O–CO–) contact intermolecularly to cancel out their polarities effectively. The length of the dimer was calculated to give 47 Å, and it agreed with the layer distance of the smectic A_d phase. Although the alkyl layer of the smectic A_d phase was sparse, the excluded volume of the alkyl chain at high temperature was large enough to supply the lack of space. After the smectic A_d phase appeared from the isotropic liquid on cooling, it retained its large hysteresis.

Introduction of an asymmetric center at the *N*-alkyl chain

Compounds *rac*-**1j**, *rac*-**1k**, (*R*)-**1k** and (*S*)-**1k** that possess a 1-methylheptyl group at the nitrogen atom were synthesized. Their behavior is shown in Table 3. All these compounds exhibited smectic A phases and the transition enthalpies of the liquid crystal–liquid transition were larger than those of compounds **1a**–**1i**. Increase of the transition enthalpies with the substitution of R^1 groups means that the difference between the molecular aggregations of the smectic A and isotropic phases became larger. It was assumed that the time-averaged dimerization in the isotropic phases of **1j**–**1k** is suppressed to some extent by the intermolecular steric repulsion between the bulky

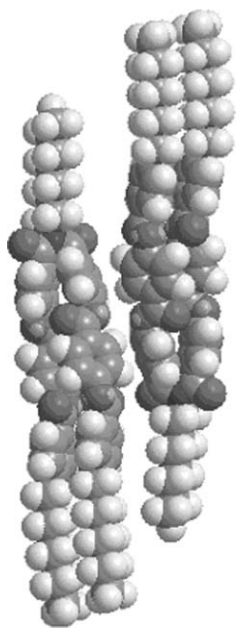


Fig. 15 Dimerization of **1e** in the smectic A_d phase. The polar parts of one molecule are near those of the other molecule to cancel out those dipoles.

R^1 (1-methylheptyl) groups. The temperature range of the liquid crystal phase of **rac-1j** was broader than that of the isomer (**1e**) on heating, and **rac-1j** did not show a clear phase transition from the smectic A to the crystal phase on cooling. The branched *N*-alkyl chain (1-methylheptyl) seems to prevent the crystallization. On the other hand, compound **rac-1k** showed a clear crystal–liquid crystal phase transition on both heating and cooling. The clearing points of chiral compounds (**R-1k** and **S-1k**) were slightly lower than that of **rac-1k**, and they did not show a clear transition from the liquid crystal to the crystal phase. Accordingly, during the crystallization

Table 3 Behavior of compounds **1j–k**

Compound	Chirality	X	Behavior ^a
rac-1j	racemic	–O–CO–	Cr $\xrightarrow{81(13.4)}$ SmA $\xleftarrow[183(-3.9)]{187(4.2)}$ I
rac-1k	racemic	–CH ₂ –CH ₂ –	Cr $\xrightarrow[68(-3.7)]{89(4.6)}$ SmA $\xleftarrow[126(-4.1)]{130(4.4)}$ I
(R)-1k	<i>R</i> -form	–CH ₂ –CH ₂ –	Cr $\xrightarrow{88(1.4)}$ SmA $\xleftarrow[127(-3.9)]{129(3.8)}$ I
(S)-1j	<i>S</i> -form	–CH ₂ –CH ₂ –	Cr $\xrightarrow{88(1.4)}$ SmA $\xleftarrow[127(-3.9)]{129(3.8)}$ I

^a The transition temperatures (°C) and enthalpies (in parentheses, kcal mol⁻¹) were determined by DSC (5 °C min⁻¹) and are given above and below the arrows. Cr, SmA, and I indicate crystal, smectic A, and isotropic phases, respectively.

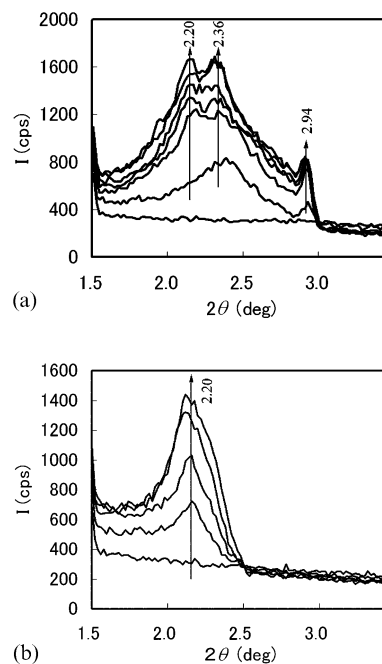


Fig. 16 (a) Growth of the liquid crystal domain of **rac-1k**. After 30 min heating at 150 °C, XRD was measured at 138, 132, 126, 120, 114, 108, and 102 °C on cooling (from the bottom to the top). The arrows indicate growth of the peaks. The temperature rate was 5 °C min⁻¹. (b) Growth of the liquid crystal domain of (**R**)-**1k**. After 30 min heating at 150 °C, XRD was measured at 132, 126, 120, 114, 108, and 102 °C on cooling (from the bottom to the top). The arrows indicate growth of the peaks. The temperature rate was 5 °C min⁻¹.

process, pairing of (**R**)-**1k** and (**S**)-**1k** may be necessary for getting the stable packing structure. Growth of the liquid crystalline domains of **rac-1k** and (**R**)-**1k** was monitored by XRD on cooling. A clear difference was observed in the growth of these peaks (Fig. 16). In the case of **rac-1k**, peaks at 2.20 (40.1 Å), 2.36 (37.4 Å), and 2.94 (30.0 Å) were observed (Fig. 16a). On the other hand, in the case of (**R**)-**1k**, only one peak at 2.20 (40.1 Å) was observed (Fig. 16b). To the best of our knowledge, this is the first example which showed a clear difference between chiral and racemic liquid crystalline compounds in interlayer interdigitations of the alkyl chains. It is thought that the peak at 2.20 originates in the layer structure of the optically pure molecules and the peaks at 2.36 and 2.94 are due to that of racemic pairs of the molecules. Accordingly, in Fig. 16a, it is assumed that the racemic domains on cooling appeared at the higher temperature and then both the racemic and the optically pure domains came out simultaneously. This might indicate that spontaneous optical resolution in a fluid liquid crystal phase²⁵ partially occurred in this system. It was supposed that the racemic pairs ((*RS*)-dimers) and chiral pairs ((*RR*)- and (*SS*)-dimers) generated by the dimerization with the large dipole–dipole interaction were organized into their own domains, respectively.

3. Conclusion

We could demonstrate that syn-parallel arrangement of two mesogenic cores by linkage with a covalent bond generated highly viscous liquid-crystal phases. It was assumed that the large dipole–dipole interaction between the “tuning fork”-shaped molecules prevented free molecular movements along their long axes. The large hysteresis in the layer distances of the smectic phase was observed because of the high viscosity and the small energy gap between the non-interdigitated and interdigitated states. From this study 1) we found that introduction of a very strong dipole along a molecular long axis remarkably decreased fluidity of the liquid crystal phase even in low

molecular-weight compounds to give high viscosity in the mesophase; 2) we could explain the probability of interdigitation using $R_{c/c}$ in the smectic A phase model, which was useful to modulate the extent of the interdigitation between the alkyl layers; 3) a clear difference between chiral and racemic liquid crystalline compounds was observed in the growth of the liquid crystal domains.

4. Experimental

The spectral data of **2a**, **2b**, **3a**, **3b**, **1a**, and **1e** were reported in our previous paper.¹⁶

An example for preparation of *N,N*-di(4-benzyloxybenzoyl)-alkylamine **2**

To a 200 ml round-bottom flask were added 4-benzyloxybenzoyl chloride (8.63 g, 35.0 mmol), *n*-dodecylamine (3.98 ml, 17.5 mmol), triethylamine (14.63 ml, 105.0 mmol), and toluene (100 ml). The mixture was then stirred at reflux for 2 days. After cooling, the solution was washed with water (100 ml), 1 N HCl (100 ml), and aqueous NaHCO₃ solution (300 ml), and dried over anhydrous MgSO₄. The solvent was evaporated under reduced pressure, and a yellow solid was obtained as the residue. The crude product was purified by silica gel chromatography eluting with chloroform to give **2c** as a white solid (3.73 g, 35.2%).

2c: mp 108.5–109.0 °C (methanol–ethyl acetate); ν/cm^{-1} (KBr) 2924, 1706, 1646, 1606, 1509, 1455, 1253, 1170, 759; δ_{H} (500 MHz, CDCl₃, TMS) 0.90 (t, 3H, $J = 6.7$ Hz), 1.25–1.43 (m, 18H), 1.82 (t, 2H, $J = 6.9$ Hz), 4.01 (t, 2H, $J = 6.9$ Hz), 5.00 (s, 4H), 6.98 (d, 4H, $J = 9.0$ Hz), 7.34 (t, 2H, $J = 9.0$ Hz), 7.38 (t, 4H, $J = 9.0$ Hz), 7.41 (d, 4H, $J = 9.0$ Hz), 8.03 (d, 4H, $J = 9.0$ Hz); δ_{C} (100.4 MHz, CDCl₃, TMS) 14.11, 22.71, 27.06, 29.10, 29.32, 29.36, 29.55, 29.65, 29.68, 31.96, 47.73, 70.24, 114.10, 127.01, 127.77, 128.20, 129.18, 130.68, 135.86, 161.10, 173.26; Elemental analysis found: C% 79.16, H% 7.89%, N% 2.07, calcd for C₄₀H₄₇NO₄: C% 79.30, H% 7.82, N% 2.31.

A typical procedure for synthesis of *N,N*-bis[4-(4-benzyloxybenzoyl)alkylamine **3**

To a 500 ml flask were added **2c** (5.00 g, 8.25 mmol), ethanol (80 ml), THF (80 ml), and 10% palladium-activated carbon (1.50 g). The mixture was stirred at room temperature for 2 h under an atmosphere of hydrogen. After filtrating off by celite, the solution was concentrated *in vacuo* to give *N,N*-di(4-hydroxybenzoyl)dodecylamine as a white solid (3.51 g). The solid was added to a 100 ml round-bottom flask, and 4-benzyloxybenzoylchloride (5.09 g, 20.6 mmol), 4-(*N,N*-dimethylamino)pyridine (2.00 g, 16.4 mmol), and THF (50 ml) were added. The mixture was stirred at room temperature for 27 h. To the solution was added ethyl acetate (50 ml), and the solution was washed with 1 N HCl (100 ml) and aqueous NaHCO₃ solution (300 ml) and dried over anhydrous MgSO₄. The solvent was evaporated under reduced pressure, and a white solid was obtained as the residue. The crude product was purified by silica gel chromatography (chloroform) to give **3c** as a white solid (2.92 g, 42.0%).

3c: mp 82.5–83.0 °C (methanol–ethyl acetate); ν/cm^{-1} (KBr) 2924, 1717, 1689, 1646, 1604, 1510, 1456, 1258, 1165, 758; δ_{H} (500 MHz, CDCl₃, TMS) 0.89 (t, 3H, $J = 7.0$ Hz), 1.27–1.45 (m, 18H), 1.83 (t, 2H, $J = 7.0$ Hz), 4.04 (t, 2H, $J = 7.0$ Hz), 5.16 (s, 4H), 7.05 (d, 4H, $J = 8.9$ Hz), 7.11 (d, 4H, $J = 8.9$ Hz), 7.38 (t, 2H, $J = 7.0$ Hz), 7.41 (t, 4H, $J = 7.4$ Hz), 7.45 (d, 4H, $J = 7.3$ Hz), 7.54 (d, 4H, $J = 8.6$ Hz), 8.11 (d, 4H, $J = 9.2$ Hz); δ_{C} (125.65 MHz, CDCl₃, TMS) 14.12, 22.70, 27.10, 29.07, 29.32, 29.37, 29.54, 29.61, 29.65, 31.94, 47.73, 70.26, 114.79, 121.62, 121.84, 127.51, 128.34, 128.76, 130.21, 132.42, 134.05, 136.08, 153.77, 163.25, 164.00, 173.48; Elemental analysis

found: C% 76.40, H% 6.28, N% 1.40, calcd for C₅₄H₅₅NO₈: C% 76.66, H% 6.55, N% 1.66.

An example for synthesis of *N,N*-bis{4-[4-(4-alkoxybenzoyloxy)-benzyloxy]benzoyl}alkylamine **1**

To a 100 ml flask were added **3c** (1.00 g, 1.19 mmol), ethanol (20 ml), THF (20 ml), and 10% palladium-activated carbon (1.00 g). The mixture was stirred at room temperature for 2 h under an atmosphere of hydrogen. After filtrating off by celite, the solution was concentrated *in vacuo* to give *N,N*-bis[4-(4-hydroxybenzoyloxy)benzoyl]dodecylamine as a white solid (0.79 g). The solid was added into a 100 ml round-bottom flask, and 4-dodecyloxybenzoylchloride (0.77 g, 2.38 mmol), 4-(*N,N*-dimethylamino)pyridine (0.80 g, 6.55 mmol), and THF (50 ml) were added. The mixture was stirred at room temperature for 2 days. To the solution was added ethyl acetate (50 ml), and the solution was washed with 1 N HCl (100 ml) and aqueous NaHCO₃ solution (300 ml) and dried over anhydrous MgSO₄. The solvent was evaporated under reduced pressure, and a white solid was obtained as the residue. The crude product was purified by silica gel chromatography (chloroform) to give **1i** as a white solid (0.89 g, 61%).

1b: yield 66.8%; white solid (methanol–ethyl acetate); ν/cm^{-1} (KBr) 2930, 1735, 1650, 1610, 1415, 1275, 1175, 780; δ_{H} (500 MHz, CDCl₃, TMS) 0.87 (t, 6H, $J = 7.0$ Hz), 0.97 (t, 3H, $J = 7.0$ Hz), 1.23–1.38 (m, 22H), 1.80 (t, 6H, $J = 6.9$ Hz), 4.03 (t, 6H, $J = 6.9$ Hz), 6.96 (d, 4H, $J = 8.6$ Hz), 7.10 (d, 4H, $J = 8.9$ Hz), 7.33 (d, 4H, $J = 8.9$ Hz), 7.52 (d, 4H, $J = 8.6$ Hz), 8.12 (d, 4H, $J = 8.9$ Hz), 8.20 (d, 4H, $J = 9.2$ Hz); δ_{C} (100.4 MHz, CDCl₃, TMS) 13.79, 14.09, 20.34, 22.64, 25.96, 29.05, 29.20, 29.30, 31.14, 31.78, 47.38, 68.37, 114.39, 120.83, 121.79, 122.16, 126.34, 130.21, 131.83, 132.40, 134.24, 153.47, 155.53, 163.62, 163.82, 164.27, 173.37; Elemental analysis found: C, 72.50% H% 6.66, N% 1.30, calcd for C₆₂H₆₇NO₁₂ (+0.5H₂O): C% 72.50, H% 6.67, N% 1.36.

Synthesis of **1j**

Synthesis of **1j** was carried with the same procedure as those of **1a–i**.

1j: white solid (methanol–ethyl acetate); ν/cm^{-1} (KBr) 2956, 2925, 2855, 1739, 1511, 1272, 1064, 760; δ_{H} (500 MHz, CDCl₃, TMS) 0.88 (t, 3H, $J = 7.1$ Hz), 0.90 (t, 6H, $J = 7.0$ Hz), 1.29–1.50 (m, 28H), 1.55 (d, 3H, $J = 7.0$ Hz), 1.83 (quint, 4H, $J = 6.9$ Hz), 1.8–1.9 (m, 1H), 2.12–2.19 (m, 1H), 4.05 (t, 4H, $J = 6.9$ Hz), 4.89 (sext, 1H, $J = 7.0$ Hz), 6.98 (d, 4H, $J = 8.9$ Hz), 7.10 (d, 4H, $J = 8.6$ Hz), 7.35 (d, 4H, $J = 8.6$ Hz), 7.52 (d, 4H, $J = 8.9$ Hz), 8.14 (d, 4H, $J = 8.9$ Hz), 8.22 (d, 4H, $J = 8.9$ Hz); δ_{C} (500 MHz, CDCl₃, TMS) 14.28, 14.31, 19.22, 22.83, 22.88, 26.21, 27.42, 29.31, 29.34, 29.44, 29.54, 31.98, 32.02, 35.21, 55.64, 68.63, 114.67, 121.13, 122.04, 122.39, 126.62, 130.38, 132.09, 132.65, 135.76, 153.68, 155.81, 163.88, 164.09, 164.51, 173.74; Elemental analysis found: C% 3.57, H% 6.83, N% 1.20, calcd for C₆₆H₇₅NO₁₂: C% 73.79, H% 7.04, N% 1.30.

Optical resolution of 2-aminooctane

In a 300 ml round-bottom flask (*S*)-mandelic acid (13.4 g, 88.1 mmol) was dissolved in ethanol (88.1 ml), and then ethyl acetate (88.1 ml) and racemic 2-aminooctane (14.8 ml, 88.1 mmol) were added. The solution was heated to dissolve the white crystals at 75 °C in a hot water bath. The solution was allowed to stand overnight. The crystals (13.2 g, 29% de) were separated by filtering with suction. The recrystallization procedure was repeated two more times to give a pure diastereomeric salt (2nd crop: 7.0 g (80% de), 3rd crop: 5.2 g (98% de)).

In a 100 ml round bottom flask, the salt (0.407 g, 2.46 mmol) was suspended in diethyl ether (20 ml), and a solution of KOH (3.04 g, 54.2 mmol) in water (30 ml) was added. The solution was stirred for 10 min at room temperature. The organic layer

was separated and dried over anhydrous MgSO_4 . The ether solution was carefully concentrated at room temperature using a rotary evaporator. The residual oil was put in a glass tube oven and the distillation gave clear oil (2-aminooctane, 0.113 g, 37%). (*S*)-2-aminooctane (98% ee): $[\alpha]_{\text{D}}^{19} +9.12^\circ$ (0.0113 g ml^{-1} , benzene), cell length: 100 mm, temperature: 19.2 °C, integration time: 60 s. (Ref. 26: (*R*)-2-octylamine, $[\alpha]_{\text{D}} -7.13^\circ$ (0.0121 g ml^{-1} , benzene)).

Determination of the enantiomeric excess. The obtained 2-aminooctane was reacted with 3,5-dinitrobenzoylchloride in the presence of triethylamine in THF at room temperature to give the corresponding amide. The enantiomeric excess of the amide was determined by HPLC using a chiral column packed in our laboratory (column: 4.6 mm \times 500 mm, solvent: hexane-isopropanol (19:1), flow rate: 2.0 ml min^{-1} , detection: 254 nm, retention time of (*R*)-isomer: 54.3 min, retention time of (*S*)-isomer: 64.0 min).²⁷

Synthesis of 1k

Synthesis of **1k** was carried according to our reported procedure.¹⁶

1k: $\nu_{\text{cm}^{-1}}$ (KBr) 2924, 2855, 1727, 1685, 1645, 1606, 1511, 1456; δ_{H} (500 MHz, CDCl_3 , TMS) 0.86 (t, 3H, $J = 6.9$ Hz), 0.89 (t, 6H, $J = 7.0$ Hz), 1.25–1.40 (m, 24H), 1.47 (quint, 4H, $J = 7.1$ Hz), 1.51 (d, 3H, $J = 7.2$ Hz), 1.75–1.85 (m, 1H), 1.81 (quint, 4H, $J = 7.1$ Hz), 2.10–2.15 (m, 1H), 2.75–2.82 (m, 8H), 4.03 (t, 4H, $J = 7.1$ Hz), 4.80 (sext, 1H, $J = 7.2$ Hz), 6.94 (d, 4H, $J = 8.1$ Hz), 6.96 (d, 4H, $J = 9.0$ Hz), 7.06 (s, 8H), 7.34 (d, 4H, $J = 8.1$ Hz), 8.12 (d, 4H, $J = 9.0$ Hz); δ_{C} (125.65 MHz, CDCl_3 , TMS) 14.07, 14.10, 18.99, 22.58, 22.65, 25.99, 27.16, 29.10, 29.22, 29.32, 31.77, 31.80, 35.01, 36.78, 37.58, 55.10, 68.35, 114.30, 121.62, 128.25, 128.36, 128.93, 129.31, 132.24, 135.99, 138.34, 145.65, 149.38, 163.54, 165.01, 174.39.

rac-1k: white solid; Elemental analysis found: C% 78.01; H% 8.12; N% 1.44, calcd for $\text{C}_{68}\text{H}_{83}\text{NO}_8$: C% 78.35; H% 8.03; N% 1.34.

(*R*)-**1k**: white solid; Elemental analysis found: C% 78.20; H% 8.09; N% 1.39, calcd for $\text{C}_{68}\text{H}_{83}\text{NO}_8$: C% 78.35; H% 8.03; N% 1.34.

(*S*)-**1k**: white solid; Elemental analysis Found: C% 78.01; H% 7.99; N% 1.51, Calcd for $\text{C}_{68}\text{H}_{83}\text{NO}_8$: C% 78.35; H% 8.03; N% 1.34.

Acknowledgements

This work was supported by Iketani Science and Technology Foundation and a Grant-in-Aid for Scientific Research (C) from the Japan Society for the Promotion of Science (JSPS) (13640571). We thank Chiba University Radioisotope Research Center for measurement of powder X-ray diffraction of the liquid crystals.

References

- Y. Lansac, M. A. Glaser and N. A. Clark, *Phys. Rev. E*, 2001, **64**, 51703/1; A. Mathis, M. Galin, J. C. Galin, B. Heinrich and C. G. Bazuin, *Liq. Cryst.*, 1999, **26**, 973; Y. E. Shapiro and A. Y. Boytsov, *Mol. Cryst. Liq. Cryst.*, 1997, **299**, 517; S. Taki and S. Kai, *Jpn. J. Appl. Phys.*, 2001, **40**, 4187.
- U. Stanislaw, R. Dabrowski, B. Gestblom and A. Kocot, *Liq. Cryst.*, 2000, **27**, 1675; J. S. Walker and J. L. Mace, *Phys. Lett. A*, 1986, **115**, 281; P. E. Cladis, *Phys. Rev. Lett.*, 1975, **35**, 48; F. Hardouin, G. Sigaud, M. F. Achard and H. Gasparoux, *Phys. Lett.*, 1979, **71A**, 347; N. H. Tinh, C. Destrade, J. Malthête and J. Jacques, *Mol. Cryst. Liq. Cryst.*, 1982, **72**, 195.
- Y. Matsunaga and S. Miyamoto, *Mol. Cryst. Liq. Cryst.*, 1993, **237**, 311; T. Akutagawa, Y. Matsunaga and K. Yasuhara, *Liq. Cryst.*, 1994, **17**, 659; T. Niori, F. Sekine, J. Watanabe, T. Furukawa and H. Takezoe, *J. Mater. Chem.*, 1996, **6**, 1231; D. R. Link, G. Natale, R. Shao, J. E. MacLennan, N. A. Koroblova and D. M. Walba, *Science*, 1997, **278**, 1924; G. Heppke and D. Moro, *Science*, 1998, **279**, 1872; D. Shen, A. Pegenau, S. Diele, I. Wirth and C. Tschierske, *J. Am. Chem. Soc.*, 2000, **122**, 1593; D. M. Walba, E. Körblava, R. Shao, J. E. MacLennan, D. R. Link, M. A. Glaser and N. A. Clark, *Science*, 2000, **288**, 2181–2184.
- S. Norvez, F.-G. Tournilhac, P. Bassoul and P. Herson, *Chem. Mater.*, 2001, **13**, 2552.
- I. A. Levitsky, K. Kishikawa, S. H. Eichhorn and T. M. Swager, *J. Am. Chem. Soc.*, 2000, **122**, 2474; K. Kishikawa, M. C. Harris and T. M. Swager, *Chem. Mater.*, 1999, **11**, 867.
- K. Kishikawa, S. Furusawa, R. Yamaki, S. Kohmoto, M. Yamamoto and K. Yamaguchi, *J. Am. Chem. Soc.*, 2002, **124**, 1597.
- C. W. Struijk, A. B. Sieval, J. J. E. Dakhorst, M. van Dijk, P. Kimkes, R. B. M. Koehorst, H. Donker, T. J. Schaafsma, S. J. Picken, A. M. van de Craats, J. M. Warman, H. Zuilhof and E. J. R. Sudhölter, *J. Am. Chem. Soc.*, 2000, **122**, 11057.
- T. Ohtake, M. Ogasawara, K. Ito-Akita, N. Nishina, S. Ujiie, H. Ohno and T. Kato, *Chem. Mater.*, 2000, **12**, 782.
- A.-J. Attias, C. Cavalli, B. Donnio, D. Guillon, P. Hapiot and J. Malthête, *Chem. Mater.*, 2002, **14**, 375; A. Rego, S. Kumar and H. Ringsdorf, *Chem. Mater.*, 1996, **8**, 1402.
- C. Nuckolls, R. Shao, W.-G. Jang, N. A. Clark, D. M. Walba and T. Katz, *Chem. Mater.*, 2002, **14**, 773.
- L. Dinescu and R. P. Lemieux, *J. Am. Chem. Soc.*, 1997, **119**, 8111.
- W. L. MacMillan, *Phys. Rev.*, 1973, **A8**, 1921.
- A. G. Khachatryan, *J. Phys. Chem. Solids*, 1975, **36**, 1055.
- J. W. Goodby, in *Handbook of Liquid Crystals*, ed. D. Demus, J. Goodby, G. W. Gray, H.-W. Spiess and V. Vill, Wiley-VCH, 1998, vol. 2A, ch.V.
- Y. Matsunaga, L. Hikosaka, K. Hosono, N. Ikeda, T. Sakatani, K. Sekiba, K. Takachi, T. Takahashi and Y. Uemura, *Mol. Cryst. Liq. Cryst.*, 2001, **363**, 51; M. Yayloyan, L. S. Bezhanova and E. B. Abrahamyan, *Ferroelectrics*, 2000, **245**, 147.
- K. Kishikawa, Y. Miwa, T. Kurosaki, S. Kohmoto, M. Yamamoto and K. Yamaguchi, *Chem. Mater.*, 2001, **13**, 2468.
- G. W. Gray and J. W. G. Goodby, in *Smectic Liquid Crystals, Textures and Structures*, Leonard Hill, London, 1984, ch. I.
- MM2 calculation: molecular modeling of compounds **1** and **2** was carried out by Chem3D (Cambridge software corporation).
- M. Nishio, M. Hirota and Y. Umezawa, *The CH/π Interaction. Evidence, Nature, and Consequences*, Wiley-VCH, New York, 1998; M. Nishio, Y. Umezawa, M. Hirota and Y. Takeuchi, *Tetrahedron*, 1995, **51**, 8665; S. Paliwal, S. Geib and C. S. Wilcox, *J. Am. Chem. Soc.*, 1994, **116**, 4497.
- K. Kishikawa, S. Tsubokura, S. Kohmoto, M. Yamamoto and K. Yamaguchi, *J. Org. Chem.*, 1999, **64**, 7568; K. Kishikawa, C. Iwashima, S. Kohmoto, K. Yamaguchi and M. Yamamoto, *J. Chem. Soc., Perkin Trans. 1*, 2000, 2217–2221.
- AM1 calculation was carried out by using WinMOPAC Ver.3 (Fujitsu, Ltd.) software. J. J. P. Stewart, *J. Comput. Chem.*, 1989, **10**, 209–220 and 221–264.
- A. J. Leadbetter, R. M. Richardson and C. N. Collings, *J. Phys.*, 1975, **36**, 37; J. E. Lydon and C. J. Coakley, *J. Phys.*, 1975, **36**, 45; D. A. Dunmur, M. R. Menterfield, W. H. Miller and J. K. Dunleavy, *Mol. Cryst. Liq. Cryst.*, 1978, **45**, 127.
- S. Diel, S. Manke, W. Weißflog and D. Demus, *Liq. Cryst.*, 1989, **4**, 301.
- The sizes of a benzene ring and an alkyl chain were calculated based on van der Waals radii. A. Bondi, *J. Phys. Chem.*, 1964, **68**, 443.
- Y. Takanishi, H. Takezoe, Y. Suzuki, I. Kobayashi, T. Yajima, M. Terada and K. Mikami, *Angew. Chem., Int. Ed.*, 1999, **38**, 2354.
- O. Mitsunobu, M. Wada and T. Sano, *J. Am. Chem. Soc.*, 1972, **94**, 697.
- K. Kishikawa, Y. Takada, K. Kawashima, S. Kohmoto, M. Yamamoto and K. Yamada, *Tetrahedron: Asymmetry*, 1996, **7**, 1733.